HHS Public Access

Author manuscript

Anat Rec (Hoboken). Author manuscript; available in PMC 2017 July 01.

Published in final edited form as:

Anat Rec (Hoboken). 2016 July ; 299(7): 840–852. doi:10.1002/ar.23352.

Comparative morphology and histology of the nasal fossa in four mammals: gray squirrel, bobcat, coyote and white-tailed deer

Karen K. Yee[1,*], **Brent A. Craven**[2], **Charles J. Wysocki**[1], and **Blaire Van Valkenburgh**[3]

[1]Monell Chemical Senses Center, 3500 Market Street, Philadelphia, PA, 19104

[2]Department of Mechanical and Nuclear Engineering, The Pennsylvania State University, University Park, PA, 16802

[3]Department of Ecology and Evolutionary Biology, UCLA, Los Angeles, CA, 90095

Abstract

Although the anatomy of the nasal fossa is broadly similar among terrestrial mammals, differences are evident in the intricacies of nasal turbinal architecture, which varies from simple scroll-like to complex branching forms, and in the extent of nonsensory and olfactory epithelium covering the turbinals. In this study, detailed morphological and immunohistochemical examinations and quantitative measurements of the turbinals and epithelial lining of the nasal fossa were conducted in an array of species that include the gray squirrel, bobcat, coyote, and white-tailed deer. Results show that much more of the nose is lined with olfactory epithelium in the smallest species (gray squirrel) than in the larger species. In two species with similar body masses, bobcat and coyote, the foreshortened felid snout influences turbinal size and results in a decrease of olfactory epithelium on the ethmoturbinals relative to the longer canine snout. Ethmoturbinal surface area exceeds that of the maxilloturbinals in all four sampled animals, except the white-tailed deer, in which the two are similar in size. Combining our results with published data from a broader array of mammalian noses, it is apparent that olfactory epithelial surface area is influenced by body mass, but is also affected by aspects of life history, such as diet and habitat, as well as skull morphology, itself a product of multiple compromises between various functions, such as feeding, vision, and cognition. The results of this study warrant further examination of other mammalian noses to broaden our evolutionary understanding of nasal fossa anatomy.

INTRODUCTION

The nasal cavity of mammals facilitates two fundamental functions: olfaction and the conservation of heat and water. Within the nasal cavity are complex turbinals, which are thin skeletal plates covered with epithelia that form an intricate passageway for airflow during breathing and active sniffing. There are three sets of paired turbinals that fill the nasal cavity, and their names reflect the bones to which they are primarily attached in the adult, viz., nasoturbinals to the nasals, maxilloturbinals to the maxillae, and ethmoturbinals to the

[*]Corresponding author: Karen Yee, Monell Chemical Senses Center, 3500 Market Street, Philadelphia, PA 19104-3308, Phone: 267-519-4823, Fax: 215-898-2084, karenyee@monell.org.

ethmoid, though the latter are also often connected to the frontal bone. The maxilloturbinals lie directly within the main path of respiratory airflow and are covered with nonsensory epithelium (respiratory, stratified or transitional). The primary functions of the maxilloturbinals are to assist in thermoregulation and water conservation during respiration (Moore, 1981; Negus, 1958). The nasoturbinals and ethmoturbinals are covered with nonsensory and olfactory epithelium (OE) and, in most mammals; there is direct airflow along the dorsal meatus into the olfactory region, where the ethmoturbinals play the primary role in olfaction (Craven et al., 2010). These three sets of turbinals are present to varying degrees in most adult mammals, with the exception of some cetaceans in which olfactory structures are reduced or lost (Berta et al., 2014).

Early studies of the mammalian nasal fossa relied on visualization of coronal sections of various noses (Negus, 1958) and quantitative measurements taken by covering the surface with paper squares or manual tracings of projected images (Adams, 1972). Advances in highresolution medical imaging, such as computed tomography (CT) and magnetic resonance imaging (MRI), have enabled three-dimensional reconstruction of the nasal fossa in various mammals (Zhao et al., 2006; Craven et al., 2007; Eiting et al., 2014, Smith et al., 2014). However, detailed histological examinations of the distribution of OE versus nonsensory epithelium within the nose are lacking for many of these species, and yet such data are essential to understanding the function of the turbinals and the nasal cavity in general.

The objective of this study is to conduct a comparative morphological and histological examination of the mammalian nasal fossa that includes identifying regions of OE and nonsensory epithelium that cover the different turbinals and septum and quantifying their surface area. The present study is a part of a larger undertaking that combines histological examination of the nasal fossa, high-resolution CT and MRI scans, anatomical reconstruction, and state-of-the-art computational modeling of nasal function to advance our understanding of mammalian respiration and olfaction. An array of species with distinct skull shapes was investigated to explore the functional significance of interspecies differences in nasal turbinal architecture. Methodology dictated that we use fresh heads for histological analysis; hence, our sample was constrained to four relatively common mammals, locally caught in Pennsylvania: the eastern gray squirrel (*Sciurus carolinensis*), bobcat (*Lynx rufus*), coyote (*Canis latrans*), and white-tailed deer (*Odocoileus virginanus*). This collection includes both carnivores (coyote, bobcat) and noncarnivores (white-tailed deer, gray squirrel), allowing for a possible comparison of nasal cavity morphology and histology with diet. In addition, it includes both short-snouted species (bobcat) and relatively long-snouted species (coyote, white-tailed deer), allowing for an examination of the possible impact of skull shape on epithelial distribution and extent. Whenever possible, we compare our results to those of prior studies on tissue distribution in the nasal cavities of various small mammals including bats, rodents, insectivores, marsupials, and primates.

METHODS

Specimens

Four, fresh, wild specimens were acquired from hunters and trappers in Pennsylvania in accordance with the regulations of the Pennsylvania Game Commission (Table 1). The head of each specimen was removed and the nose was flushed with 4% paraformaldehyde and placed in the same fixative solution for one to two weeks at 4°C. Each nasal specimen was then immersed for another two weeks in a phosphate-buffered saline (PBS) solution containing approximately 0.25% Magnevist (Bayer, Germany) for high-resolution MRI scanning. MRI scanning was performed on a 14.1-Tesla vertical Agilent system (Agilent, Santa Clara, CA) for the gray squirrel nose, and on a 7-Tesla horizontal Agilent system for all the other noses. After MRI scanning of the nasal cavity was completed, each specimen was then shipped to Monell Chemical Senses Center for histological analysis.

Tissue Preparation and Sectioning

After removing the skin and all soft tissues surrounding the nose and skull, each head was immersed in a decalcification HCl-EDTA buffer solution (Mercedes Medical) and stored at 4°C for various lengths of time (Table 1) with changes of solution every 3–4 days. The noses were then further cleaned by removing the teeth, lower jaw, orbital bones and caudal regions of the skull. The caudal portion of the brain was removed just behind the olfactory bulbs. The entire gray squirrel nose was processed for histology, whereas the bobcat, coyote and white-tailed deer noses were bisected into sagittal halves and only the right side of the nose, including the septum, was used for histological analysis. The right sides of these noses were further divided into 5 cm segments to fit into the cryostat for sectioning. The ventral portion of the white-tailed deer nose was further divided into more segments to fit onto a 75 mm by 26 mm microscope slide. All segments were immersed in 10%, 20% and 30% sucrose for cryoprotection, then embedded in M1 mounting medium (Lipshaw, Thermo), and rapidly frozen in a 100% ETOH dry ice bath. All frozen segments were coronally sectioned at a thickness of 25 μm through the entire nose. Every fifth to sixth section was collected onto Colorfrost glass slides (Mercedes Medical) and stored at −20°C.

Staining and Immunohistochemistry

For each nose, sections were selected for histological examination at intervals that varied according to the length of the nose and the integrity of the tissue section (Table 1). Sections were stained with nuclear fast red and Alcian blue which allowed for the visualization of goblet cells. To further visualize the OE, we conducted immunohistochemistry with a mouse monoclonal anti-neuronal class III β-tubulin antibody (TMJ1, Babco) as has been used to label olfactory neurons in rodents (Roskams et al., 1998), cats (Lishcka et al., 2008) and humans (Ronnett et al., 2003), suggesting reactivity of this antibody in diverse mammalian samples. This antibody was raised against microtubules derived from rat brain and recognized the epitope CEAQGPK in the carboxyl-terminus of the class III β-tubulin (Lee et al., 1990). Details of immunohistochemistry are described in Lischka et al. (2008). Briefly, tissue sections with parts of the ethmoturbinals present were blocked with Superblock (Pierce) for one hour at room temperature and incubated with 1:500 dilution of β-tubulin III antibody overnight at 4°C in a humidified chamber. After washing, tissue sections were

incubated with a secondary mouse biotinylated antibody (Vector Laboratories, Burlingame, CA, USA), followed by the avidinbiotinylated horseradish peroxidase complex ABC Elite Kit (Vector). Sections were then reacted with the chromogen diaminobenzidine (DAB; Sigma Chemicals) and 0.1% H_2O_2 for visualization.

Imaging and Morphological Analysis

Sections were imaged and captured using a SPOT RT SLIDER digital camera attached to a Nikon SMZ-U dissecting stereomicroscope with ImagePro Plus software (Media Cybernetics, v4.5). Calibrations were performed using a ruler or a stage micrometer imaged at the same magnification as the sections. Adobe Photoshop CS was used to combine individual images to create a complete tissue section. Identification of different turbinals was confirmed by comparing with MRI scans from the same nose acquired at Pennsylvania State University.

The perimeters of the septum, maxilloturbinals, nasoturbinals and summed areas of the ethmoturbinals (i.e., “endoturbinals” I through IV, frontoturbinals, and interturbinals) were manually measured in millimeters using ImagePro Plus software. In the bobcat nose, small portions of the rostral ethmoturbinals in the maxilloturbinal region were damaged during sectioning. As stated under tissue preparation, ventral parts of the white-tailed deer nose had to be cut to fit in the cryostat for tissue sectioning. As such, parts of the ethmoturbinals and septum were missing in the 16 selected, unstained and non-DAB labeled sections used for quantitative measurements. MRI scans at the level as close to the section plane based on turbinal shape and size were selected and used to help complete both ethmoturbinal and septum measurements where needed. Transparent images of MRI scans and unstained sections were overlaid and the turbinals were aligned in Photoshop.

For the gray squirrel, bobcat, and coyote, the identification of OE was based on positive labeling of β-tubulin III antibody. In the white-tailed deer, due to insufficient fixation, there was inadequate tissue and cellular integrity to distinguish individual cells and, consequently, the identification of OE was based on mucosal thickness of unstained sections. Nasal epithelium was considered to be olfactory if it was greater than 100 μm in thickness from the apical epithelial surface to the bottom of the lamina propria. The OE is much thicker than nonsensory epithelium due to the presence of more neuronal cell layers in the epithelium as well as Bowman’s glands and nerve bundles in the lamina propria. However, we likely underestimated the extent of OE in the white-tailed deer because we did not identify thinner transitional epithelium as olfactory, although it may have included a single layer of olfactory neurons. This underestimation of OE will be noted in the interpretation of our results.

The perimeter of nonsensory epithelium was calculated by subtracting the OE perimeter from the total perimeter of each section. We did not distinguish nonsensory epithelium from respiratory epithelium given the diverse array of epithelial cell types (e.g., ciliated and nonciliated, cuboidal and squamoid, and secretory cells) that would need to be identified by multiple markers (Schlage et al., 1998). If sections were unusable due to tissue folding or lifting off the slide during staining, then the next adjacent, unstained section was selected for examination. The surface area of every section was calculated as the perimeter multiplied by

the distance to the next section in millimeters, yielding a measure of the surface area between sections (Smith et al., 2007).

RESULTS

Nasal Fossa of the Gray Squirrel

Figure 1 shows a sagittal representation of the MRI scan (1A) and representative coronal sections of the gray squirrel nasal fossa at various intervals along the rostrocaudal axis (at approximately 2.9 mm (Fig 1B), 7.2 mm (Fig 1C), 15.6 mm (Fig 1D), 21.9 mm (Fig 1E), and 24.8 mm (Fig 1F) from the tip of the naris). At the rostral regions of the nasoturbinal and maxilloturbinal (Fig 1B), thin, nonsensory epithelium covers both turbinals with wide vascular spaces located underneath, in the lamina propria (Fig 1G–H). At this coronal level of the nasal fossa, the entire septum is covered with nonsensory epithelium and Alcian blue labeled goblet cells (Fig 1I). Moving along the rostrocaudal axis, branches of the naso- and maxillo-turbinals appear and increase in size (not measured) to further occupy the nasal fossa (Fig 1C), and at this level both turbinals are covered with nonsensory epithelium (Fig 1J–K) and Alcian blue labeled goblet cells cover the ventral half of the septum and the septal swell body (Fig 1L). At this position, the nasoturbinals originate caudally from the lateral wall of the nasal fossa above the origin of the maxilloturbinals.

In the next coronal section (Fig 1D), the maxilloturbinals are no longer present and the rostral ethmoturbinal emerges. The hallmarks of OE (thicker epithelium and the presence of Alcian blue labeled Bowman's glands in the lamina propria) cover the relatively simple nasoturbinal, dorsal septum, and portions of the ethmoturbinal folds (Fig 1M). β-tubulin III labeling was clearly visible along the outer surface of the ethmoturbinal folds (Fig 1N). At a higher magnification of the ethmoturbinal (Fig 1O), the cell bodies and dendrites of the olfactory sensory neurons, olfactory cilia along the apical surface of the ethmoturbinal and olfactory axonal nerve bundles in the lamina propria were all visible due to labeling with the β-tubulin III antibody. The maxillary sinus of the gray squirrel, located lateral to the nasoturbinal (Fig 1D), expands to fill the entire height of the nasal fossa after separation of the nasoturbinal from the lateral wall (Fig 1E). The olfactory bulbs appear (Fig 1F) above the dorsal meatus just below the nasal bone, as observed in other rodents (Clancy et al., 1994).

Nasal Fossa of the Bobcat

Figure 2 shows a sagittal view of the MRI scan (2A) and representative coronal sections of the bobcat nasal fossa at various intervals along the rostrocaudal axis (at approximately 11.0 mm (Fig 2B), 19.15 mm (Fig 2C), 24.3 mm (Fig 2D), 32.8 mm (Fig 2E), and 40.8 mm (Fig 2F) from the tip of the naris). In the rostral regions (Fig 2B) the nasoturbinal (Fig 2G) is covered with thin nonsensory epithelium. The septum and the maxilloturbinals are covered entirely with nonsensory epithelium, densely lined with Alcian blue goblet cells, and are highly vascularized (Fig 2H). At the next coronal section of the nasal fossa, the maxilloturbinals are folded (Fig 2C), but they do not expand to fill the nasal fossa. Instead, the maxilloturbinals are confined to the ventral half of the nasal cavity and overlaid by the rostral portion of the ethmoturbinals. Closer examination of both the ethmoturbinals (Fig 2I)

and maxilloturbinals (Fig 2J) showed that both turbinals and septum are covered with nonsensory epithelium, densely packed with Alcian blue goblet cells and still highly vascularized in the lamina propria in both turbinals.

By the next coronal section, the maxilloturbinals are no longer present (Fig 2D), and the ethmoturbinals are no longer covered with goblet cells. Moving farther caudally, the nasoturbinal scrolls dorsally and the ethmoturbinal folds become more complex (Fig 2E–F). At this caudal portion of the nasal fossa, OE covers the nasoturbinal, the dorsal septum, and the medial regions of the ethmoturbinals (Fig 2K–L). Along with the histological hallmarks of OE (Fig 2M), immunohistochemistry assisted in identifying regions of OE and nonsensory epithelium (Fig 2N). β-tubulin III mostly labels the olfactory cilia, dendrite and axonal nerve bundles and occasionally cell bodies of olfactory neurons in the bobcat (Fig 2O). The rostral-most portion of the olfactory bulb appears in the middle of the nasal fossa above the dorsal meatus and below parts of the most dorsal ethmoturbinal (Fig 2F), as has been similarly observed in other felids such as the domestic cat (Lishcka et al., 2008).

Nasal Fossa of the Coyote

Figure 3 shows a sagittal view of the MRI scan (Fig 3A) and representative coronal sections of the coyote nasal fossa at various intervals along the rostrocaudal axis (at approximately 20.4 mm (Fig 3B), 33.0 mm (Fig 3C), 54.5 mm (Fig 3D), 75.2 mm (Fig 3E), and 96.8 mm (Fig 3F) from the tip of the naris). In the rostral regions of the nasal fossa (Fig 3B), the single scroll nasoturbinal (Fig 3G) and branching maxilloturbinals (Fig 3H) are covered with nonsensory epithelium. Like the gray squirrel and bobcat, the lamina propria of both turbinals contains wide vascular spaces and are highly vascularized at this level. At the next coronal section (Fig 3C), the branches of the maxilloturbinal completely fill the nasal fossa and are covered with nonsensory epithelium and Alcian blue goblet cells (Fig 3I), as is the septum. Vascularization in the lamina propria decreases in the maxilloturbinals relative to that seen in more rostral sections.

In the next coronal section, the maxilloturbinals appear as only a small projection from the lateral wall (Fig 3D) and are covered with Alcian blue labeled goblet cells (Fig 3J–K). A portion of the frontal sinus can be seen as a cavity in the dorsal aspect of the section. The OE lines both the nasoturbinal and the dorsal half of the septum, whereas the ventral half of the septum is covered with nonsensory epithelium lined with Alcian blue labeled goblet cells. At this position, the rostral tip of the anterior-most ethmoturbinal scroll is visible and is similarly covered with Alcian blue labeled goblet cells (Fig 3L). In the next two coronal sections, the complex ethmoturbinal scrolls fill the entire nasal fossa and extend above the scrolled nasoturbinals (Fig 3E–F). In these coronal sections, OE covers both the septum and the exterior surfaces of the ethmoturbinal folds (Figure 3M–N). β-tubulin III mostly labeled the olfactory cilia and dendrites of olfactory neurons in the coyote (Fig 3O). Similar to the bobcat, the rostralmost portion of the olfactory bulb appears in the middle of the nasal fossa, above the dorsal meatus and below the most dorsal ethmoturbinals (Fig 3F).

Nasal Fossa of the White-Tailed Deer

Figure 4 shows a sagittal representation of the MRI scan (4A) and representative, unstained coronal sections of the white-tailed deer nasal fossa at various intervals along the rostral-caudal axis (at approximately 51.36 mm (Fig 4B), 79.4 mm (Fig 4C), 102.2 mm (Fig 4D), 124.3 mm (Fig 4E) and 139.4 mm (Fig 4F) from the caudal extent of the visible nose pad, which was trimmed off could fit in the cryostat). Distortion of the turbinals and septum on the representative slides occurred during embedding and freezing of the tissue. In the rostral regions of the nasal fossa, the maxilloturbinals appear as a double scroll, one ventral and one dorsal that expands caudally (Fig 4B–C). The rostral nasoturbinal appears as a single scroll from the nasals, but then becomes attached to the lateral wall caudally (Fig 4C). Similar to the other three noses, the lamina propria at these rostral levels of the deer nose is also highly vascularized. By the next coronal section (Fig 4D), the maxilloturbinals regresses into the lateral wall and the rostral tip of the ethmoturbinal emerges. Along the rostrocaudal axis, the ethmoturbinals form increasingly complex folds that fill the nasal chamber. Thicker epithelium covers the outer surface of the ethmoturbinal folds, indicating the presence of OE. The rostral portions of the olfactory bulb appear (Fig 4F) above the dorsal meatus and below the nasal bone. Higher magnifications of the ethmoturbinals illustrate the criterion that was used to determine OE from nonsensory epithelium in the white-tailed deer nose, viz., the thicker OE (Fig 4G and 4I) relative to thinner nonsensory epithelium (Fig 4H–I).

Quantitative Analysis

The total perimeter of epithelium for each coronal section in the nasal fossa, and the distribution of nonsensory epithelium and OE on each turbinal and the septum for each animal are shown from rostral to caudal in Figure 5. The relative position of the three types of turbinals and the distribution of OE along the rostrocaudal axis confirm previously reported unusual proportions of the white-tailed deer nose in which the maxilloturbinals far outdistance the caudally restricted ethmoturbinals (Ranslow et al., 2014). Unlike the gray squirrel, bobcat, and coyote, in which the maxilloturbinals are confined to the rostral half of the nose, the maxilloturbinals extend much farther caudally in the white-tailed deer. Septal surface area in all animals decreases in the caudal half of the nose due to the appearance of the nasopharyngeal duct below the septum. Nasoturbinal surface area also decreases caudally with the shortening of the septum. The ethmoturbinals are restricted to the caudal half of the nose, except in the bobcat where they extend forward into the rostral half of the nose, overlapping parts of the maxilloturbinals.

In all four species, the maxilloturbinals are lined entirely by nonsensory epithelium. Moving from rostral to caudal, OE on the septum and nasoturbinals first appears at a similar distance (about halfway) along the length of the nasal cavity in the gray squirrel, bobcat and coyote, but appears more caudally in the white-tailed deer. As expected, OE on the ethmoturbinals is localized to the caudal half of the nose. Given the very caudal position of the ethmoturbinals in the white-tailed deer, the appearance of OE is restricted to just the caudal-most 20% of the nasal cavity.

The absolute size of the turbinals, as quantified by surface area, increased with body mass in our sample (Table 2A, Fig. 6), as was found in a larger sample of carnivorans based on bony

turbinals (Green et al. 2012, Van Valkenburgh et al. 2014). However, the bobcat and coyote are similar in body mass (12 kg and 14.5 kg, respectively) and yet the coyote's septum and turbinals have much greater surface area than those of the shorter-snouted felid. The coyote has more than three times the maxilloturbinal surface area, two times both the septum and nasoturbinal surface areas, and more than two times the ethmoturbinal surface area of the bobcat. Although both animals have comparable ethmoturbinal perimeters at most cross-sectional locations, the total surface area is larger in the coyote due to its elongated nasal fossa. As expected, the white-tailed deer had the largest nasal fossa total surface area relative to the other mammals. However, unlike the other sampled animals, in which the ethmoturbinals make up greater than 60% of the total surface area, the ethmoturbinals of the white-tailed deer make up only about 40% of the total surface area and are more comparable to the maxilloturbinals in size (Fig. 7A) (Ranslow et al., 2014).

The total surface area of OE did not scale predictably with body mass (Table 2B). Although the smallest species, the squirrel, had the least OE, and the largest species, the deer, had the most OE, the intermediate sized coyote is much more similar to the deer in OE surface area than to the intermediate sized bobcat. However OE may have been underestimated in the deer due to poor tissue preservation. Despite these differences, all four species were similar in having 79% to 86% of their total OE surface area located on the ethmoturbinals as opposed to nasoturbinals or septum (Table 2C, Fig. 7B). In terms of the percent coverage of OE on the septum and each turbinal, the gray squirrel is notable in having a greater proportion of these structures covered in OE (35%–63%) than is typical of the other, larger species (13%–45%), which is consistent with previously published data on small mammals (see below). In the gray squirrel almost half of its total epithelial surface is comprised of OE, and thus the septum, nasoturbinals and ethmoturbinals were each more extensively covered in OE than in the other three species. The bobcat is unusual in having a relatively small percentage of its ethmoturbinals covered with OE, 16% as compared with the 40%-63% coverage observed in the other three species. This is due to the large rostral extensions of the ethmoturbinals in the bobcat that appear to be in the primary respiratory airflow path and are lined with nonsensory epithelium and goblet cells.

DISCUSSION

Analysis of the gray squirrel nasal fossa revealed a complex branching of the nasoturbinals and maxilloturbinals, which, to our knowledge, has not been observed in smaller rodents. In the mouse (*Peromyscus maniculatus sonoriensis*, Adams 1972), rat (*Rattus norvegicus*, Schreider and Raabe, 1981), and hamster (*Mesocricetus auratus*, Adams and McFarland, 1972; Clancy et al., 1994), the nasoturbinals and maxilloturbinals are scrolls. The complex branching in the squirrel nose implies increased respiratory surface area and more efficient heat and water regulation. Similarly, in the chinchilla (*Chinchilla langiera*), a larger rodent with an average body mass of 600–800 g (Jurcisek et al., 2003), more intricate branching of the maxilloturbinals was observed, though less complex than the gray squirrel. Although the percent of nonsensory epithelium in the smaller Syrian hamster nose (Clancy et al., 1994) is similar to the gray squirrel, without examining a broader sample of rodents, it is unclear whether the greater complexity of the maxilloturbinals in both the gray squirrel and chinchilla, relative to the smaller rodents, is due to larger body size or environmental

adaptations. Chinchillas live at high altitudes and gray squirrels exist in cool, temperate environments, both of which likely increase thermoregulatory demands.

The structure and location of the turbinals in the carnivores are similar to those previously observed in members of their respective families. Like other short-snouted *Felidae* (e.g., domestic cat, African wild cat, cheetah, and puma), the ethmoturbinals of the bobcat extended rostrally into the maxillary region of the nasal fossa, lying above the smaller maxilloturbinals (Lischka et al., 2008; Van Valkenburgh et al., 2004, 2014). Furthermore, the rostral extensions of the ethmoturbinals are lined with nonsensory epithelium and goblet cells that may serve to compensate for the reduced maxilloturbinal surface area. Whether these anatomical and morphological compensations also occur in other short snouted carnivores requires further examination. As observed in other *Canidae* (e.g., domestic dog, grey fox and grey wolf), the complex branches of the maxilloturbinals of the coyote fill the entire cavity at the maxillary level of the nasal fossa and do not overlap the ethmoturbinals (Craven et al., 2007; Van Valkenburgh et al., 2004 and 2014).

Considering the morphology of the turbinals, in the present study we observe each of the types of turbinals identified by Negus (1958), namely single-scroll, double-scroll, folded, and branching. The gray squirrel, bobcat, and coyote all possess branching maxilloturbinals, whereas the white-tailed deer possesses maxilloturbinals of the double-scroll type. This agrees with the turbinal designations of Negus (1958) for members of each of these families, except for the gray squirrel, as Negus (1958) identifies other members of the Sciuridae family (red squirrel and flying squirrel) as having folded maxilloturbinals. The squirrel and coyote both possess single- and double-scroll ethmoturbinals, as does the bobcat, with the exception of the rostral ethmoturbinal extensions, which appear to lie in the main respiratory flow path and are of the branching type. The white-tailed deer, on the other hand, possesses folded ethmoturbinals that are more convoluted than the single- and double-scroll ethmoturbinals of the other animals, which, as observed by Ranslow et al. (2014), provides a larger surface area for olfaction in a compact space.

Comparisons with Other Mammals

Using both their own data on primates and previously published data, Smith et al. (2012 and 2014) explored the scaling of the total surface area of OE with body mass in 16 species of small mammals. The mean OE area percentages of these various mammalian species grouped by order (e.g. Chiroptera) including the ones from this study are listed in Table 3. The size range of species for which they had data was limited, ranging from less than 5 g (*Sorex cinereus*, common shrew) to 350 g (*Hemiechinus auritus*, long-eared hedgehog), but nevertheless they found a significant positive relationship between $\log_{10}$ OE area and $\log_{10}$ body mass that was negatively allometric (slope = 0.4, $r^2 = 0.28$, $p<0.05$). We extended their analysis, adding the four species that are the focus of this paper, as well as two felids (Pang et al. (2016)), thus extending the upper size limit to 62 kg (Fig. 8A). The relationship between the two variables remained significant and strong ($r^2= 0.76$, $p<0.05$), but the slope of the line increased to 0.55 (95% C.I. = 0.41–0.68), which is not significantly different from isometric. Species falling somewhat below the line that appear to have reduced OE for their size include two of the primates (the white-tufted ear and pygmy marmosets, *Callithrix*

jacchus and *Cebuella pygmaea*, respectively), and the two domestic cats (*Felis catus*). The reduced quantity of OE in the domestic cats relative to the bobcat is intriguing and might reflect a reduced need for olfaction due to domestication, but this should be verified with a larger sample size. The coyote is the most prominent outlier above the line with markedly greater OE area for its body mass. An enlarged OE surface area and presumably enhanced olfactory ability may be typical of many canids given that previous work has shown that canids tend to have large ethmoturbinals relative to other similar sized carnivorans (Green et al. 2012).

The squirrel is distinctive in having a much greater percentage of its nasal cavity covered in OE than our other three species, but it appears that this is not unusual given its small body size. A plot of the percent of the total surface area of the nasal cavity lined with OE for various mammals for which we could find data shows that this percentage declines rapidly with body mass (Fig. 8B). In the five mammals larger than 1 kg, OE covers less than 30% of the nasal cavity, whereas for mammals below that threshold, the percent ranges from as little as 15% (pygmy marmoset) to nearly 70% (common shrew).

There is considerable scatter in the relationship between percent OE coverage and body mass, and some of this may have functional significance. For example, among the four bats sampled, two are insectivorous brown bats (*Myotis lucifugens, M. blythii*) and have less of their nasal cavity covered in OE relative to the carnivorous greater false vampire bat (*Megaderm lyra*) and Jamaican fruit-eating bat (*Artibeus jamaicensis*). Both *Myotis* species have reduced total OE relative to the other two bats as well (Fig. 8A), and this has been suggested to reflect a reduced reliance on olfaction in the insectivores (Bhatnagar and Kallen 1975). Similarly, Larochelle and Baron (1989) observed that the semi-aquatic shrew, *Neomys fodiens*, had a relatively reduced total olfactory surface area, relative to terrestrial species in the genera *Sorex, Blarina*, and *Crocidura*, and it appears that this is accompanied by a reduction in the percentage of the nasal cavity that bears OE. Semi-aquatic habits are well known to be associated with a reduced reliance on olfaction in mammals (Pihlstrom 2008, Van Valkenburgh et al. 2011). Finally, among the carnivorans, both the bobcat and domestic cats contrast with the coyote in having much less of their nasal cavity cloaked in OE, and this likely reflects a reduced emphasis on olfaction in the felids.

Smith et al. (2014) found an interesting difference in the distribution of OE between two marmoset species (*Callithrix jaachus, Cebuella pygmaea*) and the lesser mouse lemur (*Microcebus murinus*). Both of the marmosets had more than 70% of their OE located on surfaces other than the ethmoturbinals, such as paranasal spaces and the septum. By contrast, the lemur split the distribution of OE nearly evenly between the ethmoturbinals and other surfaces. Smith et al, (2014) suggested that this contrast in OE distribution was due to differences in skull shape. The marmosets have very reduced snouts and closely-set eyes relative to the mouse lemur, limiting the space available for the ethmoturbinals. Following from this, it might be expected that the most short-snouted species within our sample of four larger mammals, the bobcat, would also show a greater distribution of OE on structures other than the ethmoturbinals. This redistribution does not seem to be the case as all four of our species have between 78% and 86% of their OE located on their ethmoturbinals. Nevertheless, it is true that, of the four, the bobcat has the greatest percentage of OE

distributed elsewhere, and differs considerably from the similar-sized coyote. This difference suggests that as in primates, skull structure also could be playing a role among carnivorans in determining OE spatial distribution, but our sample size is too small to be certain.

All of the foregoing observations regarding the comparative analyses would benefit greatly from a broader sampling of mammals, especially in the size ranges of 1 kg to 7 kg, and 15 kg to 100 kg for which we have almost no data. The comparisons made herein and in Smith et al. (2014) strongly suggest OE surface area is in part determined by body mass, but that it is also affected by aspects of life history, such as diet and habitat, as well as skull morphology, itself a product of multiple compromises between various functions, such as feeding, vision, and cognition. Our progress in understanding tissue distribution within the nasal cavity has been slowed by the difficulty of applying traditional histological approaches of sectioning and staining to larger species, as evidenced here by the problems with the deer. However, new techniques such as iodine enhanced computed tomography (Gignac and Kley 2014) of entire heads are on the horizon and should allow for more rapid assessment of tissue distributions in a broad array of species.

Results of this study showed the importance of detailed measurements of OE and turbinals in understanding how nasal turbinal size and epithelial surfaces compensate for changes in body size, snout length, and habitat. Our results will be combined with future studies utilizing MRI data to generate anatomical reconstructions of the nasal cavity in the same specimens (e.g., Ranslow et al., 2014), which will be used in computational simulations of nasal airflow and odorant deposition (e.g., Craven et al., 2009, 2010; Lawson et al., 2012). Taken together, these studies will add to our understanding of the mammalian nose and reveal the influence of interspecies differences in nasal morphology on respiratory and olfactory function.

Acknowledgments

We thank T. Neuberger at the Pennsylvania State University for the MRI data and A. Quigley, A. Ranslow, J. Richter, C. Rumple, and A. Rygg for technical assistance in processing and segmenting the MRI scans. T.D. Smith generously shared his data with us for the comparative analyses. The paper was much improved by the suggestions of T.D. Smith and an anonymous reviewer. This work was supported by National Science Foundation Grants to C.J. W. (IOS-1118852), B.A.C (IOS-1120375) and B.V.V. (IOS-1119768). All morphological and histological analyses and microscopy were performed at the Monell Histology and Cellular Localization Core, which is supported, in part, by funding from the NIH-NIDCD Core Grant P30DC011735.

BIBLIOGRAPHY

Adams DR. Olfactory and non-olfactory epithelia in the nasal cavity of the mouse, *Peromyscus*. Am J Anat. 1972; 133:37–50. [PubMed: 5008884]

Adams DR, McFarland LZ. Morphology of the nasal fossae and associated structures of the hamster (*Mesocricetus auratus*). J Morphol. 1972; 137:161–180. [PubMed: 4113181]

Berta A, Ekdale EG, Cranford TW. Review of the cetacean nose: form, function, and evolution. Anat Rec (Hoboken). 2014; 297:2205–2215. [PubMed: 25312374]

Bhatnagar KP, Kallen FC. Quantitative observations on the nasal epithelia and olfactoryinnervation in bats. Acta Anat. 1975; 91:272–282. [PubMed: 1146482]

Clancy AN, Schoenfeld TA, Forbes WB, Macrides F. The spatial organization of the peripheral olfactory system of the hamster. Part II: receptor surfaces and odorant passageways within the nasal cavity. Brain Res Bull. 1994; 34:211–241. [PubMed: 8055348]

Craven BA, Neuberger T, Paterson EG, Webb AG, Josephson EM, Morrison EE, Settles GS. Reconstruction and morphometric analysis of the nasal airway of the dog (*Canis familiaris*) and implications regarding olfactory airflow. Anat Rec (Hoboken). 2007; 290:1325–1340. [PubMed: 17929289]

Craven BA, Paterson EG, Settles GS, Lawson MJ. Development and Verification of a High-Fidelity Computational Fluid Dynamics Model of Canine Nasal Airflow. J Biomech Eng. 2009; 131:091002. [PubMed: 19725691]

Craven BA, Paterson EG, Settles GS. The fluid dynamics of canine olfaction: unique nasal airflow patterns as an explanation of macrosmia. J R Soc Interface. 2010; 7:933–943. [PubMed: 20007171]

Eiting T, Smith TD, Dumont ER. Olfactory epithelium in the olfactory recess: a case study in new world leaf-nosed bats. Anat Rec (Hoboken). 2014; 297:2105–2112. [PubMed: 25312368]

Gignac PM, Kley NJ. Iodine-enhanced micro-CT imaging: methodological refinements for the study of the soft-tissue anatomy of post-embryonic vertebrates. J Exp Zool B Mol Dev Evol. 2014; 322:166–176. [PubMed: 24482316]

Green P, Van Valkenburgh B, Pang B, Bird D, Rowe T, Curtis A. Respiratory and olfactory turbinal size in canid and arctoid carnivorans. J Anat. 2012; 221:609–6021. [PubMed: 23035637]

Jurcisek JA, Durbin JE, Kusewitt DF, Bakaletz LO. Anatomy of the nasal cavity in the chinchilla. Cells Tissues Organs. 2003; 174:136–152. [PubMed: 12835577]

Larochelle L, Baron G. Comparative morphology and morphometry of the nasal fossae of four species of North American shrews (Soricinae). Am J Anat. 1989; 186:306–314. [PubMed: 2618929]

Lawson MJ, Craven BA, Paterson EG, Settles GS. A Computational Study of Odorant Transport and Deposition in the Canine Nasal Cavity: Implications for Olfaction. Chem Senses. 2012; 37:553–566. [PubMed: 22473924]

Lee MK, Rebhun LI, Frankfurter A. Posttranslational modification of class III β-tubulin. Proc Natl Acad Sci USA. 1990; 87:7195–7199. [PubMed: 2402501]

Lischka FW, Gomez G, Yee KK, Dankulich-Nagrudny L, Lo L, Haskins ME, Rawson NE. Altered olfactory epithelial structure and function in feline models of mucopholysaccharidoses I and VI. J Comp Neurol. 2008; 511:360–372. [PubMed: 18803239]

Moore, WJ. The mammalian skull. Cambridge: Cambridge University Press; 1981.

Negus, VE. The comparative anatomy and physiology of the nose and paranasal sinuses. London: Livingstone; 1958.

Pang B, Yee KK, Lischka FW, Rawson NE, Haskins ME, Wysocki CJ, Craven BA, Van Valkenburgh B. The influence of nasal flow on respiratory and olfactory epithelial distribution in felids. J Exp Biol. 2016 (2016).

Pihlstrom, H. Comparative anatomy and physiology of chemical senses in aquatic mammals. In: Thewissen, JGM.; Nummela, S., editors. Sensory Evolution on the Threshold. Berkeley: University of California Press; 2008. p. 95-109.

Ranslow AN, Richter JP, Neuberger T, Van Valkenburgh B, Rumple CR, Quigley AP, Pang B, Krane MH, Craven BA. Reconstruction and morphometric analysis of the nasal airway of the white-tailed deer (*Odocoileus virginianus*) and implications regarding respiratory and olfactory airflow. Anat Rec (Hoboken). 2014; 297:2138–2147. [PubMed: 25312370]

Roskams AJI, Cai X, Ronnett GV. Expression of neurons-specific beta-III tubulin during olfactory neurogenesis in the embryonic and adult rat. Neuroscience. 1998; 83:191–200. [PubMed: 9466409]

Ronnett GV, Leopold D, Cai X, Hoffbuhr KC, Moses L, Hoffman EF, Naidu S. Olfactory biopsies demonstrate a defect in neuronal development in Rett's syndrome. Ann Neurol. 2003; 54:206–218. [PubMed: 12891673]

Schlag WK, Bulles H, Friedrichs D, Kuhn M, Teredesai A. Cytokeratin expression patterns in the rat respiratory tract as markers of epithelial differentiation in inhalation toxicology. I. Determination of normal cytokeratin expression patterns in nose, larynx, trachea, and lung. Toxicol Pathol. 1998; 26:324–343. [PubMed: 9608639]

Schreider JP, Raabe OG. Anatomy of the nasal-pharyngeal airway of experimental animals. Anat Rec (Hoboken). 1981; 200:195–205.

Smith TD, Bhatnagar KP, Rossie JB, Docherty BA, Burrows AM, Cooper GM, Mooney MP, Siegel MI. Scaling of the first ethmoturbinal in nocturnal strepsirrhines; olfactory and respiratory surfaces. Anat Rec (Hoboken). 2007; 290:215–237. [PubMed: 17525938]

Smith TD, Eiting TP, Bhatnagar KP. A quantitative study of olfactory, non-olfactory, and vomeronasal epithelia in the nasal fossa of the bat *Megaderma lyra*. J Mammal Evol. 2012; 19:27–41.

Smith TD, Eiting TP, Bonar CJ, Craven BA. Nasal morphometry in marmosets: loss and redistribution of olfactory surface area. Anat Rec (Hoboken). 2014; 294:2093–2014. [PubMed: 25312367]

Van Valkenburgh B, Theodor J, Friscia A, Pollack A, Rowe T. Respiratory turbinates of canids and felids: a quantitative comparison. J. Zoo London. 2004; 264:281–293.

Van Valkenburgh B, Curtis A, Samuels JX, Bird D, Fulkerson B, Meachen-Samuels J, Slater G. Aquatic adaptations in the nose of carnivorans: Evidence from the turbinates. J Anat. 2011; 218:298–310. [PubMed: 21198587]

Van Valkenburgh B, Pang B, Bird D, Curtis AC, Yee K, Wysocki C, Craven BA. Respiratory and olfactory turbinals in feliform and caniform carnivorans: the influence of snout length. Anat Rec (Hoboken). 2014; 297:2065–2097. [PubMed: 25312365]

Zhao K, Dalton P, Yang GC, Scherer PW. Numerical modeling of turbulent and laminar airflow and odorant transport during sniffing in the human and rat nose. Chem Senses. 2006; 31:107–118. [PubMed: 16354744]

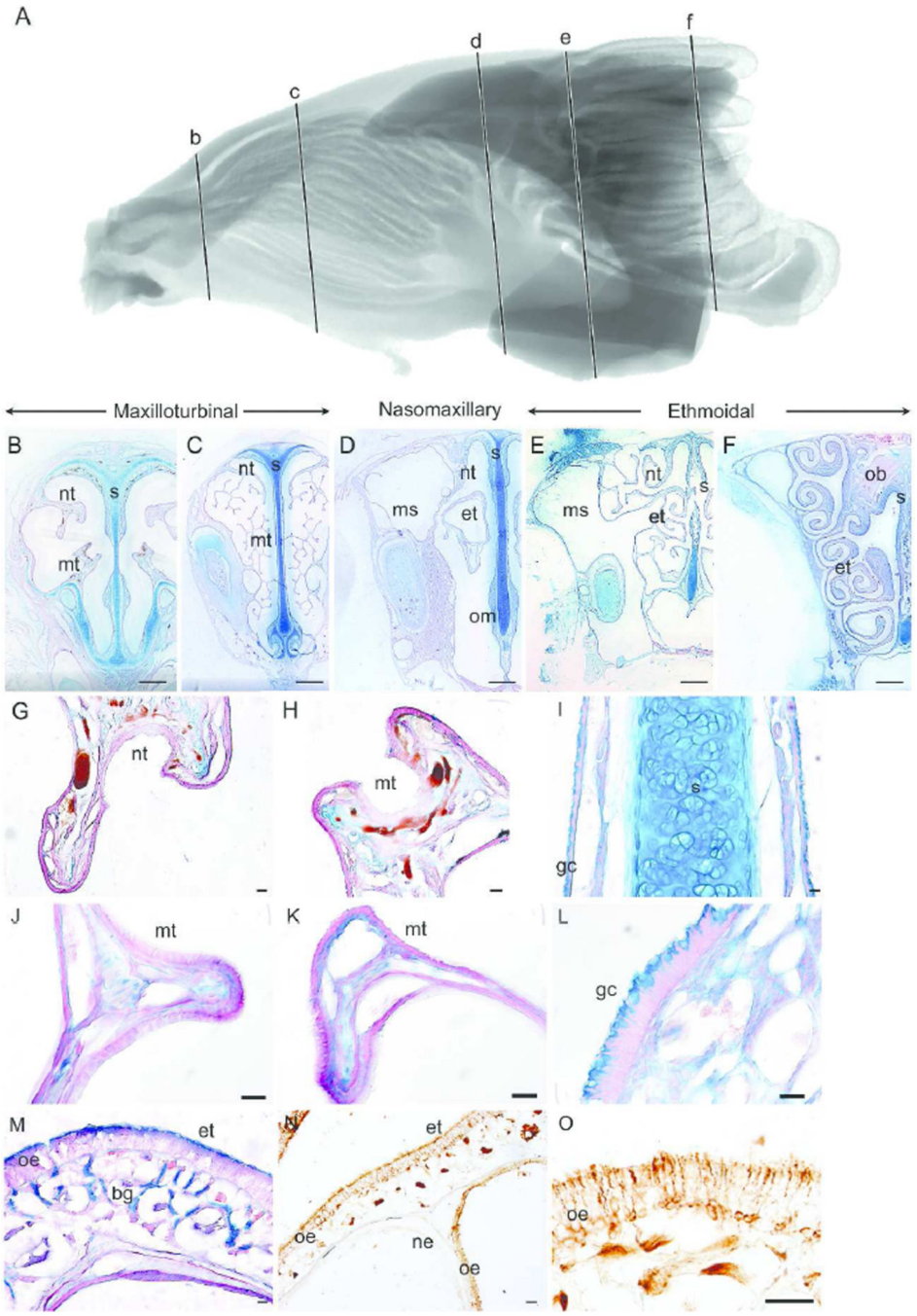

Figure 1.

Epithelial lining of the gray squirrel nasal fossa. Sagittal view of segmented MRI scans of the gray squirrel nasal airway showing five coronal sections (b–f) selected for morphological and histological representation (A). The five coronal sections along the rostrocaudal axis illustrate the maxilloturbinal (B–C), nasomaxillary (D) and ethmoturbinal (E–F) regions of the gray squirrel nasal fossa. Magnified views show the nonsensory epithelium lining the nasoturbinal (G), maxilloturbinal (H, J–K), septum (I) and septal swell body (L). In the nasomaxillary region, the dorsal half of the septum and the outside of the ethmoturbinal

folds (M) are covered with olfactory epithelium, which was identified with immunohistochemisty (NO). nt = nasoturbinal; mt = maxilloturbinal; s = septum; et = ethmoturbinal; ms = maxillary sinus; om = organ of Masera; ob = olfactory bulb; gc = goblet cell; oe = olfactory epithelium; bg = Bowman's gland; ne = nonsensory epithelium. Scale bar: B–F = 1 mm; G–O = 50 μm.

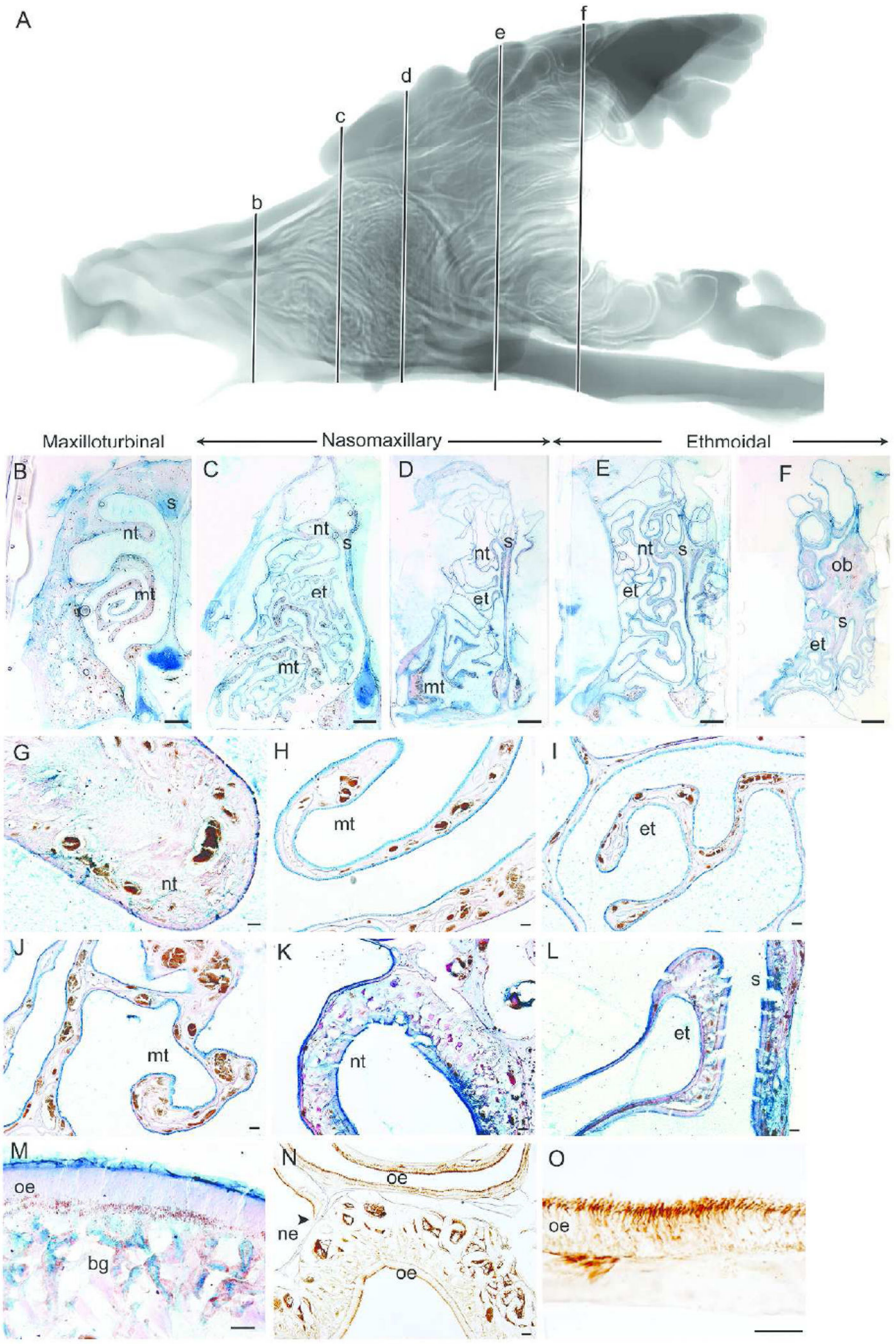

Figure 2.

Epithelial lining of the bobcat nasal fossa. Sagittal view of segmented MRI scans of the bobcat nasal airway showing five coronal sections (b–f) selected for morphological and histological representation (A). The five coronal sections along the rostrocaudal axis illustrate the maxilloturbinal (B–C), nasomaxillary (D) and ethmoturbinal (E–F) regions of the bobcat nasal fossa. Magnified views show the nasoturbinal (G), maxilloturbinal (H, J) and ethmoturbinal (I) covered with nonsensory epithelium and packed with Alcian blue labeled goblet cells at rostral regions of the nasal fossa. Olfactory epithelium covered the

nasoturbinal (K), septum (L), and ethmoturbinal (L) in more caudal regions and had the characteristic epithelial thickness and Bowman's glands in the lamina propria (M) and labeled with β-tubulin III antibody (N–O). nt = nasoturbinal; mt = maxilloturbinal; s = septum; et = ethmoturbinals; ob = olfactory bulb; oe = olfactory epithelium; bg = Bowman's gland; ne = nonsensory epithelium. Scale bar: B–F = 2 mm; G–L, N = 100 μm; and M, O = 50 μm.

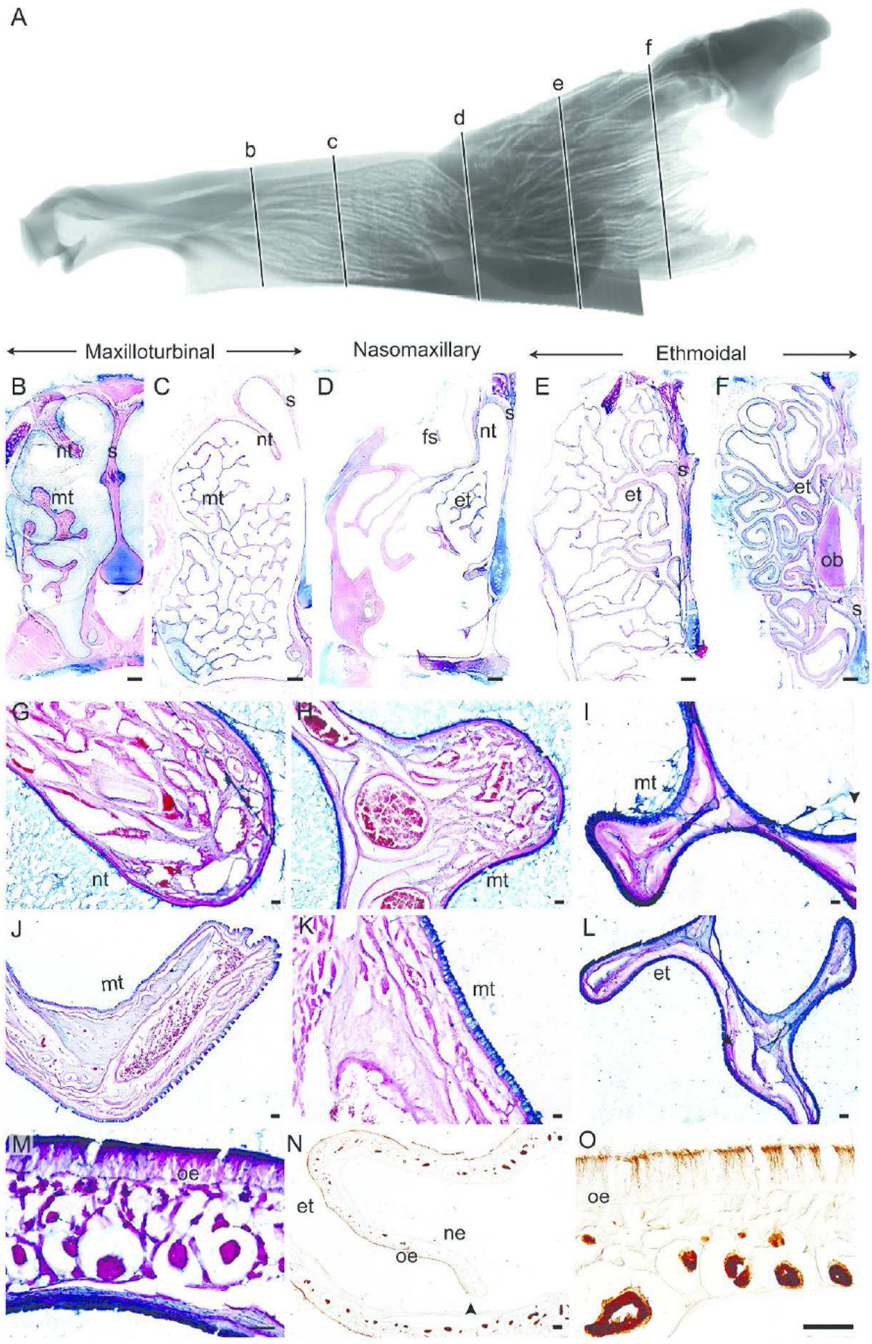

Figure 3.

Epithelial lining of the coyote nasal fossa. Sagittal view of segmented MRI scans of the coyote nasal airway showing five coronal sections (b–f) selected for morphological and histological representation (A). The five coronal sections along the rostrocaudal axis illustrate the maxilloturbinal (B–C), nasomaxillary (D) and ethmoturbinals (E–F) regions of the coyote nasal fossa. Nonsensory epithelium covered the nasoturbinal (G), maxilloturbinal (H–K), and ethmoturbinal (L) at the rostral regions. Thick olfactory epithelium (L), clearly labeled with β-tubulin antibody (N–O), covered the septum, nasoturbinal, and ethmoturbinal

at the caudal regions of the nasal fossa. nt = nasoturbinal; mt = maxilloturbinal; s = septum; et = ethmoturbinal; fs = frontal sinus; ob = olfactory bulb; oe = olfactory epithelium; ne = nonsensory epithelium. Scale bar: B–F = 2 mm; G–L, N = 100 μm; and M, O = 50 μm.

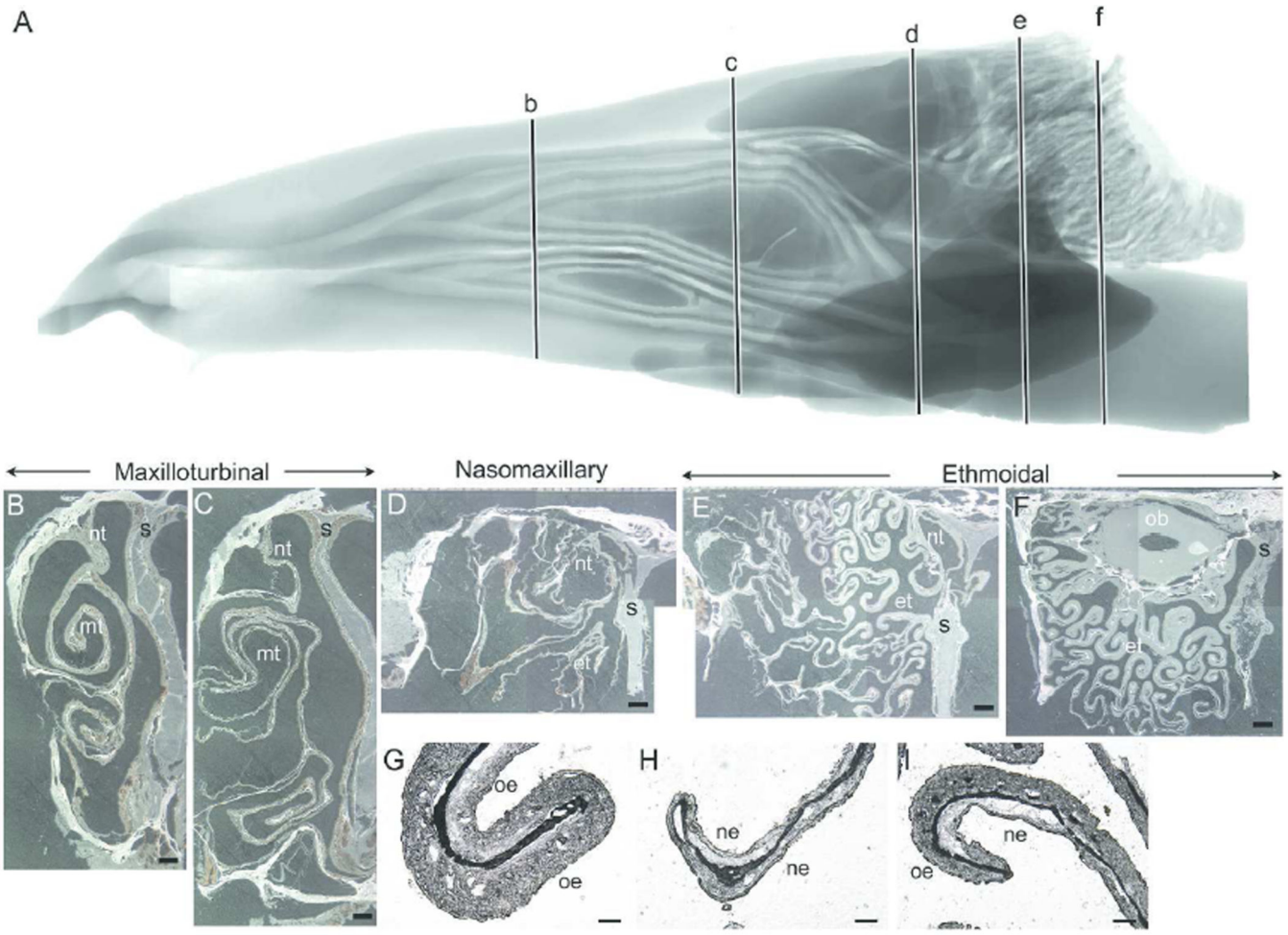

Figure 4.

Nasal fossa of the white-tailed deer. Sagittal view of segmented MRI scans of the white-tailed deer nasal airway showing five coronal sections (b–f) selected for morphological and unstained histological representation (A). Representative coronal sections along the rostrocaudal axis illustrating the maxilloturbinal (B–C), nasomaxillary (D) and ethmoturbinal (E–F) regions of the white-tailed deer nasal fossa. The double scroll of the maxilloturbinal fills the rostral regions of the nasal fossa. In the caudal regions, the ventral half of the nasal fossa, beneath the ethmoturbinals, is occupied by the nasopharyngeal meatus (not shown). Representative coronal sections are montages created from individual images and the slight differences observed between these individual images are due to the unstable light intensity of the dissecting stereomicroscope's light source when these images were captured. Higher magnification of unstained ethmoturbinal showed examples of the thicker olfactory epithelium compared with the thinner nonsensory epithelium (G–I). nt = nasoturbinal; mt = maxilloturbinal; s = septum; et = ethmoturbinals; ob = olfactory bulb; oe = olfactory epithelium; ne = nonsensory epithelium. Scale bar: B–F = 2 mm; G–I = 200 μm.

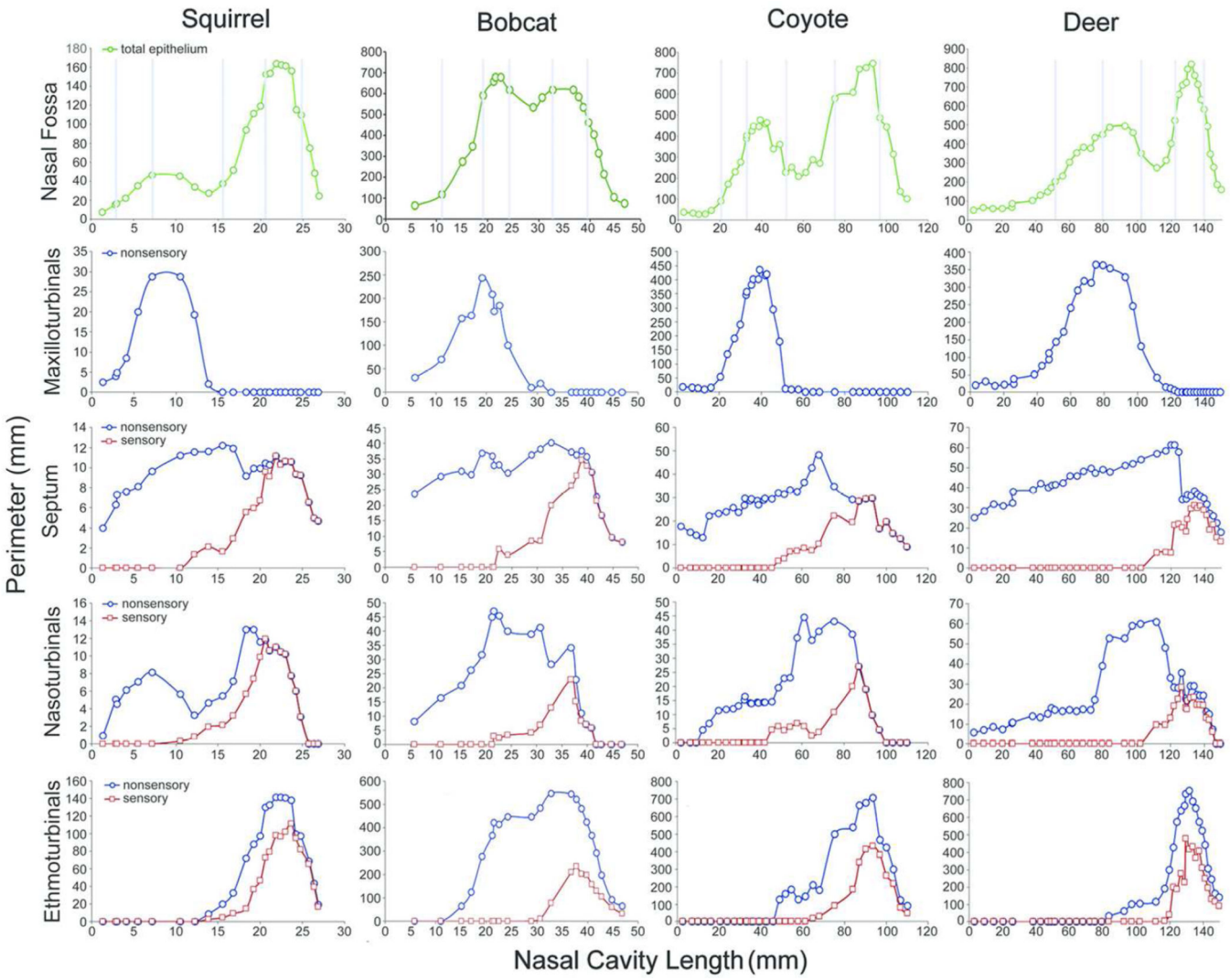

Figure 5.

Plots of the nasal fossa perimeters. The total epithelial perimeter (green) of the entire nasal fossa for each animal is shown on the first row. Light blue vertical lines indicate where along the rostrocaudal axis each coronal section shown in Figs 1–4 is located in each nose. In the remaining rows, the perimeters of nonsensory (blue) and olfactory epithelium (red) on each turbinal and septum at various intervals are plotted for each animal along the rostrocaudal axis of the nose.

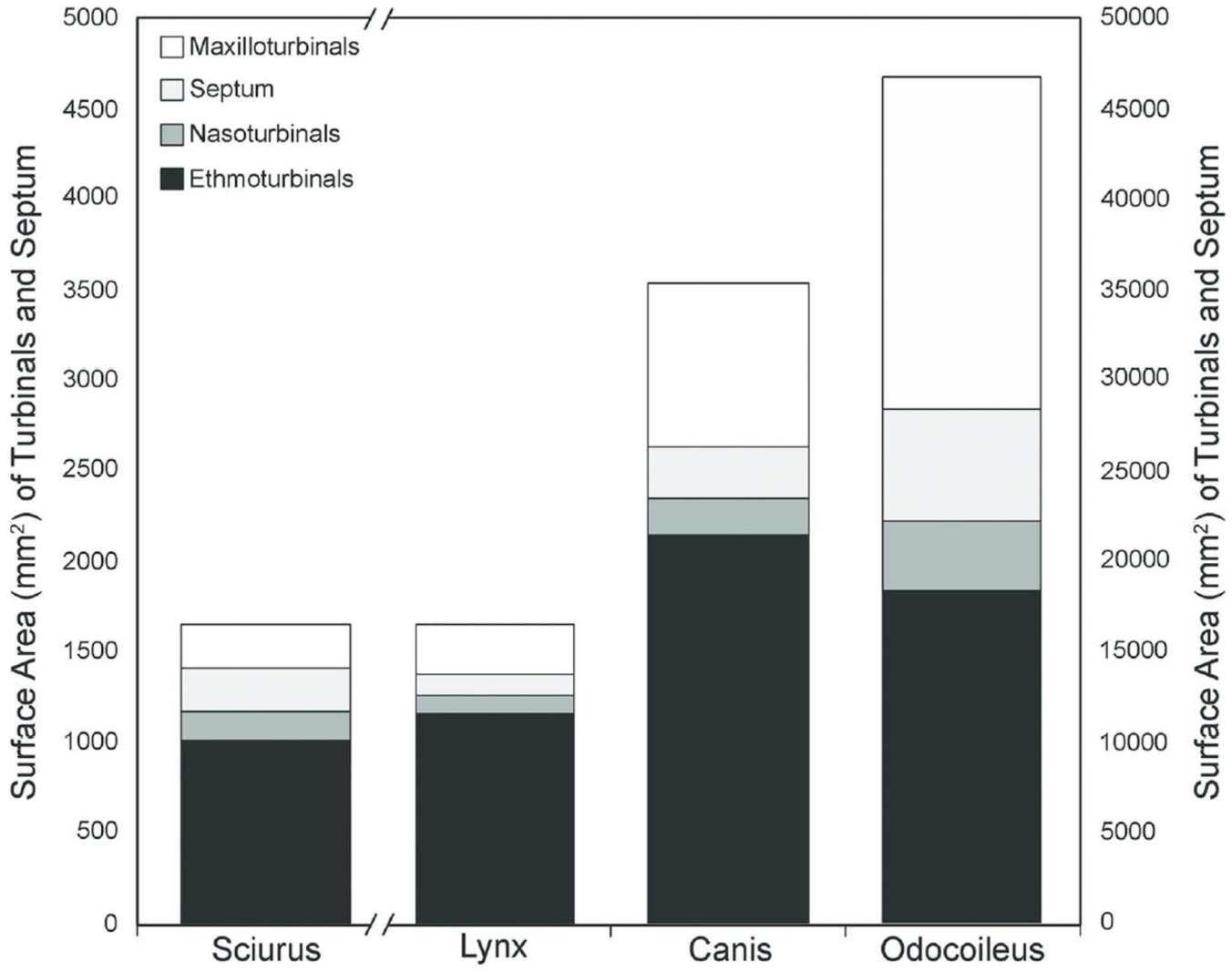

Figure 6.

Measured surface area of turbinals and septum for each species. The left Y-axis depicts the scale range for *Sciurus* and the right Y-axis depicts the scale range for the other three mammals. Scale is in mm^2.

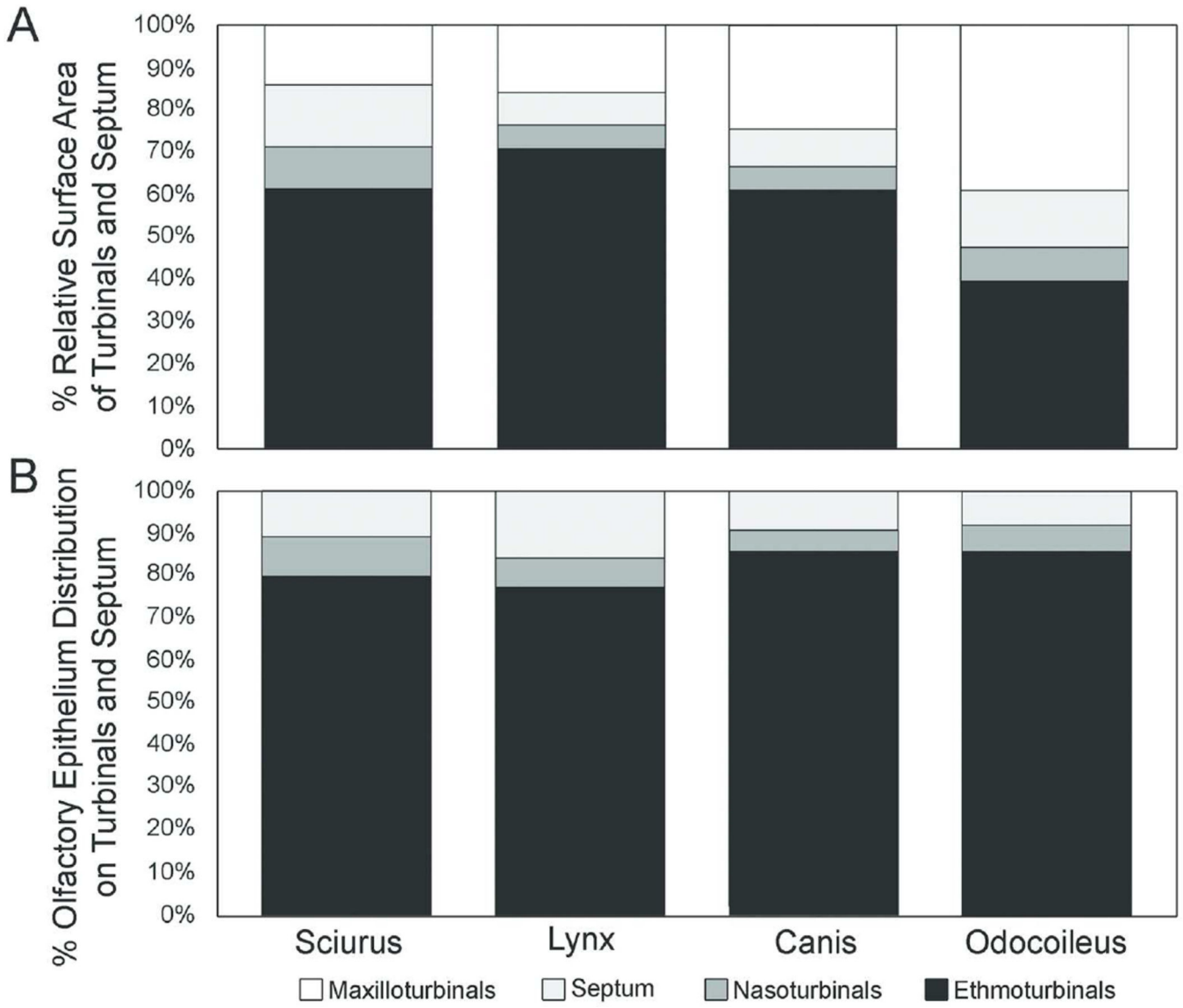

Figure 7.

Percentage of relative surface area of turbinals and septum (A) and olfactory epithelial distribution on turbinals and septum (B).

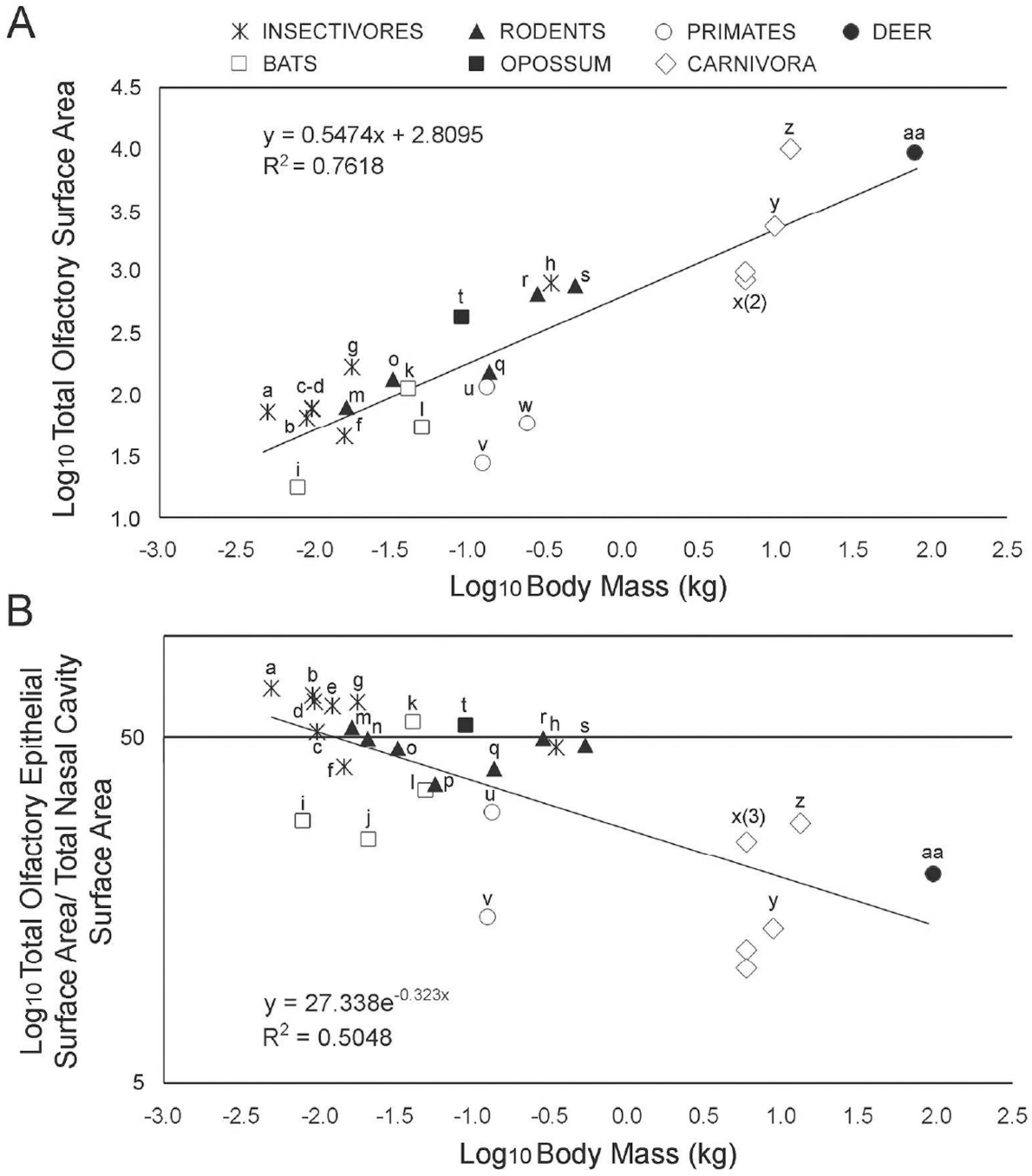

Fig 8.

Comparison between different mammalian species. Scatter plot with best-fit least squares regression lines for total olfactory epithelium surface area relative to body mass (A) and the ratio of OE surface area divided by total nasal fossa surface area relative to body mass (B). All measurements were $\log_{10}$-transformed. Data for the white tailed deer, coyote, bobcat, and eastern gray squirrel are from this study; the data for two domestic cats are from Pang et al. (2016); the data for *Blarina bervicauda* are from Larochelle and Baron (1989); all other data are from Smith et al. (2012, 2014). Species coded as follows: a) *Sorex cinereus*, b)

Sorex fumeus, c) *Sorex palustris*, d) *Crocidura leucodon*, e) *Crocidura russula*, f) *Neomys fodiens*, g) *Blarina brevicauda*, h) *Erinaceus aurtius*, i) *Myotis lucifugus*, j) *Myotis blythii*, k) *Artibeus jamaicansis*, l) *Megaderma lyra*, m) *Peromyscus maniculatus*, n) *Cleithironomys sp*, o) *Mus musculus*, p) *Microtis gregalis*, q) *Mesocricetus auratus*, r) *Rattus norvegicus*, s) *Sciurus carolinensis*, t) *Monodelphis domestica* u) *Microcebus murinus*, v) *Cebuella pygmaeus*, w) *Callithrix jacchus*, x) *Felis catus*, y) *Lynx rufus*, z) *Canis latrans*, and aa) *Odocoileus virginianus*.

Table 1

Description of mammals from which nasal samples were obtained, length of time for decalcification prior to histological processing and distance between sections selected for analysis.

Taxon	Sex	Mass (kg)	Decalcification (wks)	Distance (mm)
Sciurus	female	0.418	3	1.0–1.5
Lynx	female	12.0	6	2.0–4.0
Canis	female	14.5	12	2.0–2.5
Odocoileus	male	62.0	18	3.0–3.5

Table 2

Calculated total surface area of each turbinal and septum and calculated total surface area of olfactory epithelium (OE) covering each turbinal.

A) Surface area in mm^2 (% of total)

	Sciurus	Lynx	Canis	Odocoileus
all turbinals +septum	1646.12 (100%)	16444.57 (100%)	35266.23(100%)	46739.44 (100%)
maxilloturbinals	234.94 (14.3%)	2649.05 (16.3%)	8854.25 (25.1%)	18324.56 (39.2%)
septum	244.35 (14.8%)	1245.01 (7.6%)	2980.12 (8.5%)	6264.21 (13.4%)
nasoturbinals	167.96 (10.2%)	989.55 (6.0%)	2012.62 (5.7%)	3855.07 (8.3%)
ethmoturbinals	998.87 (60.7%)	11560.96 (70.1%)	21419.25 (60.7%)	18295.58 (39.1%)

B) Sensory epithelial surface area in mm^2 (% of total epithelial area on the structure)

	Sciurus	Lynx	Canis	Odocoileus
total OE in nasal fossa	786.78 (47.8%)	2333.93 (14.2%)	10065.53 (28.5%)	9533.76 (20.4%)
OE on septum	84.34 (34.5%)	369.82 (29.7%)	946.99 (31.8%)	787.09 (12.6%)
OE on nasoturbinals	73.66 (43.9%)	155.33 (15.7%)	494.94 (24.6%)	575.23 (14.9%)
OE on ethmoturbinals	628.78 (62.9%)	1808.78 (15.6%)	8623.6 (40.3%)	8171.47 (44.7%)

C) Distribution of OE

	Sciurus	Lynx	Canis	Odocoileus
% OE on septum	10.7%	15.8%	9.4%	8.3%
% OE on nasoturbinals	9.4%	6.7%	4.9%	6.0%
%OE on ethmoturbinals	79.9%	77.5%	85.7%	85.7%

Table 3

Comparison of mean percentage of total nasal fossa area covered by olfactory epithelium in seven mammalian orders. Data are from the four focal species used in this study as well as from Smith et al. (2012, 2014).

Order (number of species)	% OE area ± SD	Range
Marsupials (1)	54.8	–
Rodentia (6)	46.7 ± 5.8	37.0 – 54.0
Chiroptera (5)	37.6 ± 12.0	25.5 – 55.9
Carnivora (3)	22.6 ± 7.5	14.2 – 28.5
Lipotyphlans (5+)	54.3 ± 11.0	41.2 – 69.3
Artiodactyla (1)	20.4	–
Primate (2)	22.9 ± 10.9	15.2 – 30.6